Geomechanics and Engineering, *Vol. 39, No. 6 (2024) 563-577*
https://doi.org/10.12989/gae.2024.39.6.563

Experimental study on mechanical properties of the non-equal-size rock-coal composite specimens

Dawei Yin[1], Yu Sun[2], Xiaotian Yuan*[2], Xuelong Li[1], Shaojun Xuan[3] and Zhen Zhang[3]

[1]*Mine Disaster Prevention and Control-Ministry of State Key Laboratory Breeding Base, Shandong University of Science and Technology, Qingdao, China*
[2]*College of Energy and Mining Engineering, Shandong University of Science and Technology, Qingdao, China*
[3]*Shandong Kangge Energy Technology Co., Ltd., Jining 272000, China*

(*Received March 23, 2024, Revised November 22, 2024, Accepted December 17, 2024*)

Abstract. The residual coal pillar and roof strata of strip mining in coal mine constitute a joint bearing body, which can be simplified into " T " shaped unequal size rock-coal combination sample in laboratory test. In this paper, the uniaxial compression test of the composite specimen is carried out to explore its mechanical properties. The results show that both sides of the specimen sandstone can share part of the load. As the width ratio h of rock and coal increases, the peak load of the composite increases, but the effect is limited. When h reaches 2.0, the " bending " deformation on both sides of the sandstone is prominent, which aggravates the damage of the combined coal sample and reduces the bearing capacity. The acoustic emission characteristic signal of the rock-coal composite sample can be divided into four stages : calm, fluctuating rise, growth and steep increase. With the increase of h, the acoustic emission signal is more obvious, the failure time of the composite sample is prolonged, and the failure mode of the sample is changed from spalling failure to spalling-ejection mixed failure.

Keywords: bending deformation; coal-rock interactions; dynamic b-value; failure mechanism; rock-coal assemblage

1. Introduction

Strip mining is widely used in China because it can effectively control overburden movement and surface subsidence, protect surface buildings (structures) and ecological environment (Liu *et al.* 2022, Gao *et al.* 2016). During coal mining, the coal seam and the roof and floor strata coexist synergistically, and the remaining coal pillars and the roof strata form a new bearing structure after the coal resources are mined, As shown in Fig. 1(a), part of the coal pillars are able to better control the movement and deformation of the overlying strata within a certain period of time. However, as time goes by, the remaining elastic core area of the internal elasticity of part of the long term load-bearing coal pillars is too small to continue to support the overlying strata, the coal pillars will be destroyed, destabilized and collapsed (Atsushi Hani 2017, Chen *et al.* 2018). Once the coal pillar is destabilized, it will cause a chain reaction of large-scale destabilization of the coal pillar group, and even cause damage to the adjacent rock strata, inducing the overall destabilization of the coal-rock interbedding, which seriously threatens the production safety and property loss of the coal mine (Kabiesz *et al.* 2015). The existing research results show that (Lei *et al.* 2023, Li *et al.* 2022, Vinay *et al.* 2022, Li *et al.* 2024, Zhang *et al.* 2023, Ma *et al.* 2020), coal pillar instability disaster is the result of the overall destabilization of the structural body under the action of overburden load. Therefore, it is of great theoretical significance to study the mechanical properties of the "rock-coal" composite structure and predict the deformation and failure of the underground coal based on it (Liu *et al.* 2018), in order to ensure the stability of the coal-rock composite structure and realize the prevention and control of the coal pillar instability disaster and the gas outburst disaster.

For a long time, domestic and foreign scholars have carried out a lot of research work on the structure of "roof-coal pillar", "coal pillar-floor" and "roof-coal pillar-floor", simplifying the interlayer methods between roof and floor strata and coal pillar, and forms rock-coal composite by bonding or free superposition of roof rock and coal specimen with binder. Petukhov (1979) for the first time analyzed the stability of coal and roof or floor rock composite samples. Chen *et al*. (2019a, b, 2018) carried out uniaxial compression tests on rock-coal composite specimens from different loading rates and joints, and revealed the differences in the mechanical properties of the composite and its progressive failure mechanism. Chen *et al*. (2019) obtained mechanical parameters such as uniaxial compressive strength (UCS), modulus of elasticity and full-scale stress-strain curve by experimental and numerical methods, studied the deformation and damage behaviours of coal-rock assemblages under uniaxial compression, and analysed in detail the evolution of internal cracks based on X-ray computed tomography (CT) observations and acoustic emission (AE) locations. Zuo *et al*. (2019) compared and analyzed the acoustic emission characteristics and failure characteristics of pure coal, pure rock and coal rock in the process of failure. Sinha *et al*.

*Corresponding author, Master student
E-mail: yxt1228353914@163.com

Copyright © 2024 Techno-Press, Ltd.

ISSN: 2005-307X (Print), 2092-6219 (Online)

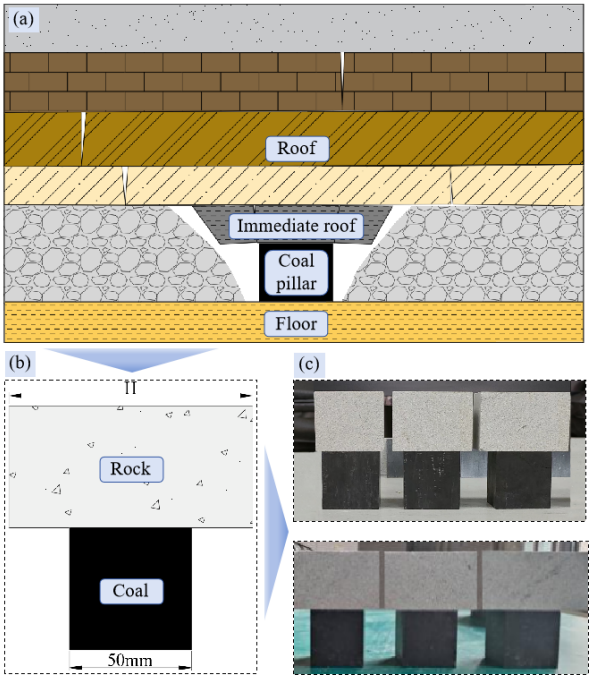

Fig. 1 Roof-coal pillar structure diagram

(2021) developed hypothetical granite column models with aspect ratios (W / H) of 1, 2 and 3. By matching the stress-strain response of the bonded block model (BBM) with the stress-strain curve from the FLAC3D model to constrain the input parameters, the column damage mechanism and rock-support interaction in block to sparse fractured rock masses were studied. Ma *et al*. (2022) conducted a series of uniaxial compression tests on cracked coal-rock assemblage specimens and analysed the strength and deformation properties, acoustic emission characteristics and damage processes of specimens with different crack inclinations. Marasanov *et al.* (2019) introduced the theoretical and experimental results of the acoustic emission signal energy spectrum of the precursor model of the deformation process in the medium with microstructure, explained the causal relationship between the acoustic emission signal and the microstructure defect. The obtained results can observe the dynamic development of the defect and provide the prediction of the material state. Xue *et al.* (2022) studied the failure characteristics of coal-rock combination (CRCB) and revealed the mechanism of rock burst. In order to explore the accumulation layer of rock burst energy in coal-rock system, Chen *et al*. (2022) constructed mechanical model of the coal-rock composite based on the structural characteristics and mechanical properties of the coal-rock, and deduced the calculation formula of energy distribution of coal-rock composite. Liu *et al*. (2021) conducted uniaxial and triaxial compression tests at 8, 16 and 25 MPa on coal rock boulders using MTS815 to investigate the strength and deformation characteristics of coal rock under different circumferential pressures. Jiang *et al*. (2024) carried out uniaxial compression and dynamic disturbance tests on shaly sandstone, coal and soft rock-coal composite samples using a creep disturbance dynamic impact loading test system. The damage characteristics of soft rock-coal composite under dynamic disturbance were analyzed by using acoustic emission system combined with sample failure characteristics, energy evolution and sample waveform signals. Hu *et al.* (2023) carried out the unloading confining pressure test of coal-rock comosite under different pressure rates, and analysed the damage, deformation, and strength characteristics of the coal-rock assemblage by observing the stress-strain curves of the assemblage in the test. Jin *et al.* (2017) investigated the highly positive correlation between the plastic stress of loaded coal and AE (acoustic emission) characteristic parameters through uniaxial experiments. Zhao *et al.* (2016) used PFC2D software to carry out uniaxial/biaxial compression simulation tests on coal-rock composite specimens, and explored the influence of interface angle on the failure characteristics and mechanism of coal-rock composite. Zhao *et al.* (2015) constructed jointed rock mass materials with different inclinations under different stress conditions by PFC numerical simulation, and analyzed the mechanical properties and fracture characteristics of the rock mass.

The above studies provide an important theoretical basis for recognizing the mechanical properties and failure instability of the roof-coal pillar structure, but most of the studies are based on the standard cylindrical rock-coal, coal-rock, rock-coal-rock and other binary and ternary composite specimens. However, in engineering practice, there are differences between rock width and coal pillar width in roof caving, and the current research on this aspect is relatively scarce. In view of this, according to the characteristics of the composite structure of rock strata and coal pillars with different widths, six groups of rock-coal composite specimens with different sizes were prepared.

With the help of acoustic emission system and three-dimensional full-field strain measurement system (XTDIC), the uniaxial compression test of rock-coal composite samples was carried out. The peak load, deformation failure characteristics and acoustic emission evolution characteristics of unequal size rock-coal composite were analyzed, and then the internal mechanism of bearing failure was revealed. The research results can provide some theoretical reference for the prevention and control of coal pillar instability disaster.

2. Specimen preparation and test methods

2.1 Specimen preparation

After the exploitation of coal resources, the width of the direct roof of the coal pillar is irregular, thus forming an unequal size “ roof-coal pillar” composite structure (Fig. 1(a)). The mechanical properties of the composite structure determine its supporting capacity to the overlying rock. In order to study its bearing capacity, it is simplified as a “T” -shaped unequal-size rock-coal composite sample (Fig. 1(b)). Six groups of samples with rock-coal width ratios h (H/50) of 1.0,1.2,1.4,1.6,1.8 and 2.0 (Fig. 1(c)) were prepared, and uniaxial compression tests were carried out in the laboratory. In order to reduce the influence of the

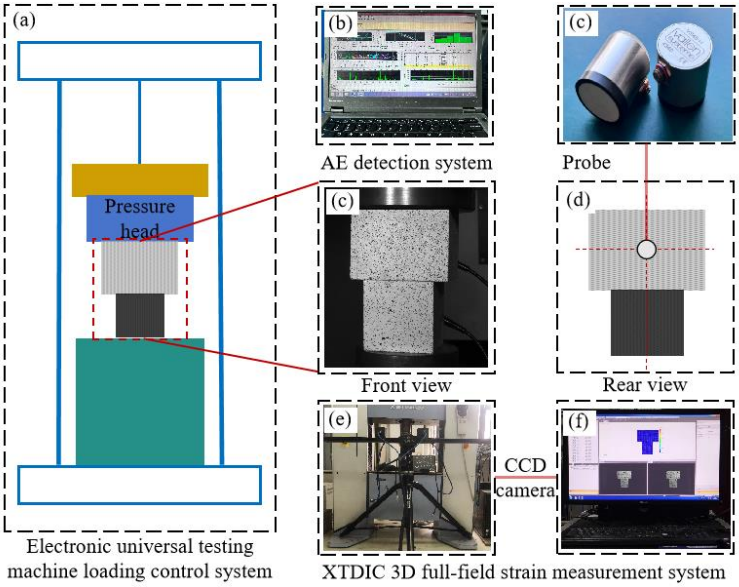

Fig. 2 Test control and monitoring system

discreteness of coal samples on the test results, all sandstone and coal samples were taken from the same rock and coal.

The preparation steps of the rock-coal composite specimens are as follows :

Firstly, the coal block is cut into a cube sample with an edge length of 50 mm by a cutting machine. The rock blocks were cut into square cylinder samples with a height of 50,60,70,80,90 and 100 mm, and three rock samples of each size were prepared.

Secondly, the six end faces of the sample are polished by a grinding stone machine. It is necessary to ensure that the end faces are smooth. The non-parallelism of the corresponding end faces is controlled in the range of less than 0.05 mm, and the axial difference should not be greater than 0.25 °.

Finally, the sandstone and coal samples were bonded to each other by epoxy resin AB glue (as shown in Fig. 1(c)), and the samples were divided into six groups : A, B, C, D, E and F, corresponding to the above different width ratios.

2.2 Test equipment and monitoring methods

The test control and monitoring system consists of a loading system, an acoustic emission system and a three-dimensional full-field strain measurement system (Fig. 2). In order to reduce the time error and facilitate the processing and analysis of the test data, the loading system, the acoustic emission system and the three-dimensional full-field strain measurement system are synchronized during the test.

The loading system adopts Shimadzu AG-X250 electronic universal testing machine (Fig. 2(a)). The testing machine is driven by AC motor servo. The loading mode adopts double screw structure. The equipment has good stability and high precision. It can realize conventional compression, tensile and other mechanical tests. The maximum load can reach 250 kN. During the test, the displacement loading control was adopted, and the loading rate was 0.005 mm/s until the specimen was destroyed (Yin *et al.* 2022, Lv *et al.* 2024).

The MISTRAS series PCI-2 acoustic emission system (Fig. 2(b)) was used to monitor the acoustic emission signals of rock-coal composite specimens with different sizes during uniaxial compression failure in real time. Vaseline was applied between the sensor (Fig. 2(c)) and the specimen for coupling to ensure that the acoustic emission signals could be well received by the sensor. The XTDIC three-dimensional full-field strain measurement system (Fig. 2(f)) was used to monitor the deformation characteristics of rock-coal composite specimens with different sizes during uniaxial compression. During the test, the speckle pattern of rock-coal composite specimens was collected by CCD industrial camera (Fig. 2(e)) of the digital speckle strain measurement system, and the acquisition frequency was 3 frames/s.

3. Mechanical properties of rock-coal composite

3.1 Peak load analysis of rock-coal composite

The load-time curves of monolithic sandstone, coal specimen and non-equal-size rock-coal composite specimens are shown in Fig. 3. When h is less than 1.8, the peak load of the composite specimen shows an increasing trend with the increase of h. When h=1.8, the peak load is the largest, which is 136.34 kN; when h=2.0, the peak load of the assemblage is the smallest, which is 58.12 kN. The variation of load with time can be roughly divided into three stages: initial compaction stage, elastic stage and instability failure stage. At the initial stage of loading, the initial microcracks inside the composite specimen slowly closed, and the load-time curve showed a nonlinear growth. As the load increases, the composite specimen enters the linear elastic deformation stage and continues to accumulate

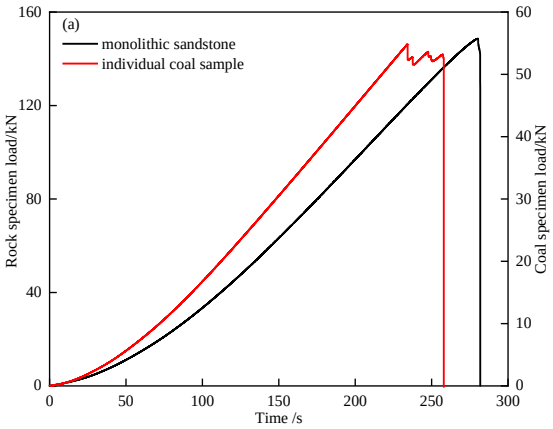

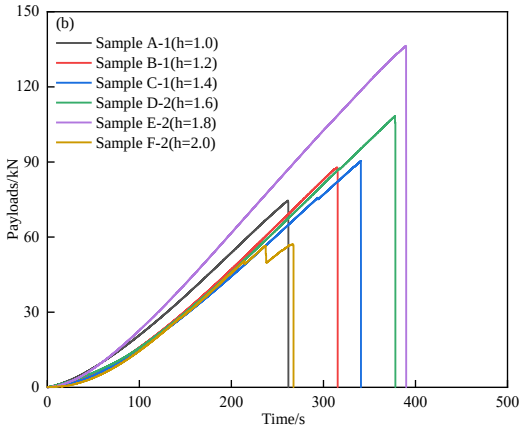

(a) Monolithic sandstone, coal specimens (b) Non-equal-sized rock-coal assemblage specimens

Fig. 3 Load-time curves for monolithic sandstone, coal and rock-coal composite specimens

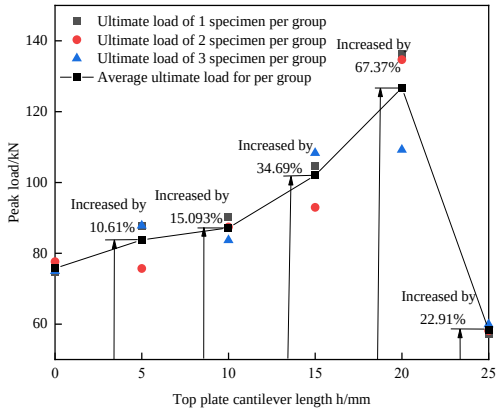

Fig. 4 The relationship curve between peak load and h of non-equal-size rock-coal composite specimens

energy, and the microcracks inside the composite continue to initiate and expand. When the axial load reaches the ultimate load that the internal structure of the composite specimen can bear, the specimen enters the stage of instability and failure, and its bearing capacity continues to decline, and the macroscopic performance is the instability and failure of the specimen. The plastic deformation of the rock-coal combination sample in the pre-peak stage is not significant, and the post-peak stage is brittle failure.

The uniaxial compression test results of monolithic sandstone, coal specimen and non-equal-size rock-coal composite specimens are shown in Table 1, and the peak load versus h curves of non-equal-size rock-coal assemblage specimens are given in Fig. 4. From Table 1 and Fig. 4, the average peak loads of monolithic sandstone and coal samples were 150.38 kN and 54.21 kN, respectively, and the peak loads of rock-coal assemblage samples were larger than that of monolithic coal samples and smaller than that of monolithic sandstone. The average peak load of group A was 75.73 kN, compared with group A, the average peak load of group B, C, D and E increased by 10.61%, 15.09%, 34.69% and 67.37%, respectively. The variation range of peak load of rock-coal composite showed an increasing trend, and the average peak load of group F decreased by 22.91%. With the increase of h, the peak load of the composite specimens showed a trend of increasing and then decreasing.

The peak load of the rock-coal composite sample is between the peak load of the single coal sample and the peak load of the sandstone, which indicates that compared with the single coal sample, the increase of the peak load of the composite sample is not only due to the size effect of the coal sample, but also the interaction between the sandstone and the coal sample.

When the rock-coal width ratio h is 1.0 ~ 1.8, the peak load of the rock-coal combination shows an increasing trend. This is due to the compression deformation of sandstone and coal samples during the axial load loading process. With the increase of the bearing area of the structure on both sides of the sandstone, it can share the load borne by the coal sample as the main bearing structure, thus inhibiting the damage of the axial load to the coal sample (main bearing body), and thus improving the overall bearing capacity of the combination sample. As h further increases to 2.0, the peak load of the rock-coal composite decreases, which is due to the limited contribution of the structural load on both sides of the sandstone to the axial load. At this time, the “bending effect” between coal and rock is highlighted, which will have a significant deterioration effect on the combination and aggravate the degree of instability and failure of the combination. The specific analysis is shown in Chapter 4.

3.2 Deformation and failure characteristics of the composite body

The failure process of the composite is also the process of interaction between the micro-cracks within the rock and coal, and its damage pattern can effectively reflect the load history experienced by the assemblage specimen, so it is of great significance to analyze the damage pattern of the assemblage specimen. Specimens A-3, B-3, C-2, D-1, E-2 and F-3 were selected to analyze the progressive failure characteristics of the rock-coal composite specimens. Fig. 5 shows the final failure diagram of the non-equal-size rock-coal composite specimens.

Table 1 Uniaxial compression test results of monolithic sandstone, coal samples and rock-coal composite specimens

Groups	h	Value type	Peak load/kN
Monolithic sandstone	-	Minimum ~ maximum	142.88 ~ 155.66
		Average value	150.38
Individual coal specimen	-	Minimum ~ maximum	49.08 ~ 58.73
		Average value	54.21
Group A	1.0	Minimum ~ maximum	74.59 ~ 77.62
		Average value	75.73
Group B	1.2	Minimum ~ maximum	75.70 ~ 87.80
		Average value	83.76
Group C	1.4	Minimum ~ maximum	83.68 ~ 90.37
		Average value	87.16
Group D	1.6	Minimum ~ maximum	92.95 ~ 108.30
		Average value	102.00
Group E	1.8	Minimum ~ maximum	109.21 ~ 136.34
		Average value	126.74
Group F	2.0	Minimum ~ maximum	57.10 ~ 59.92
		Average value	58.38

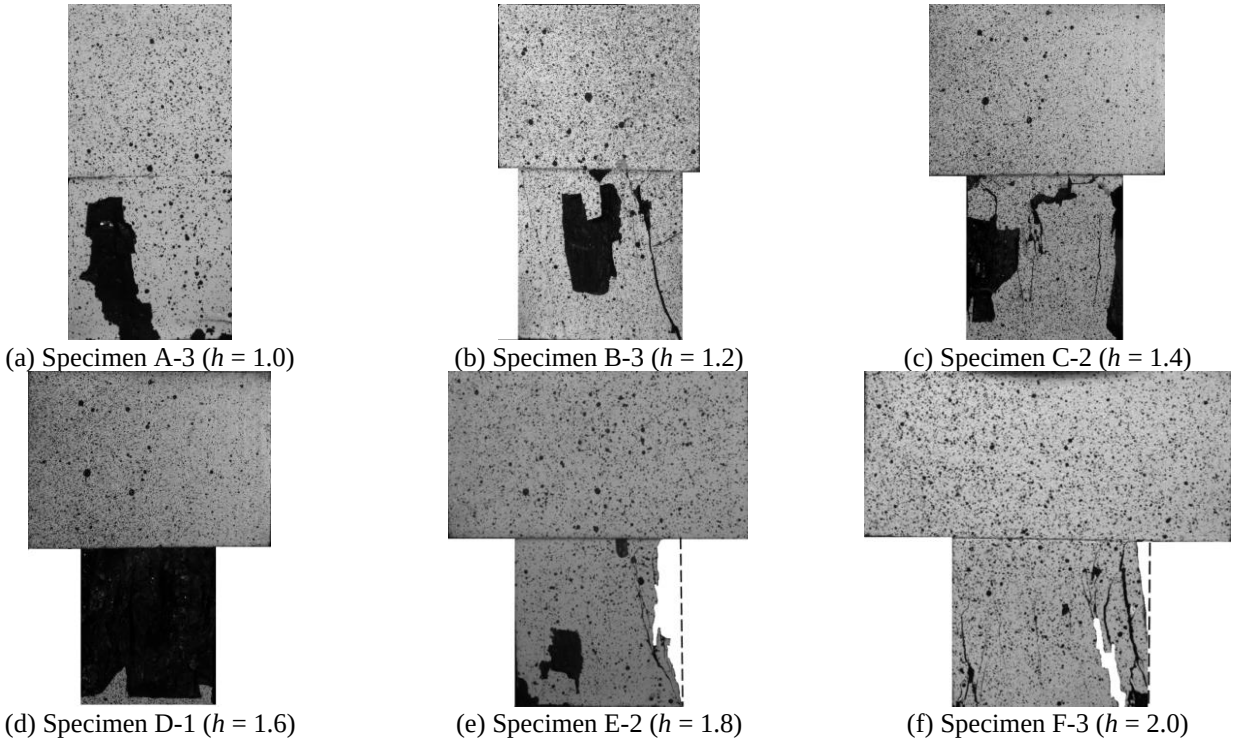

(a) Specimen A-3 (h = 1.0) (b) Specimen B-3 (h = 1.2) (c) Specimen C-2 (h = 1.4)

(d) Specimen D-1 (h = 1.6) (e) Specimen E-2 (h = 1.8) (f) Specimen F-3 (h = 2.0)

Fig. 5 Final failure diagram of non-equal-size rock-coal composite specimen

It can be seen from Fig. 5 that the coal body of the composite specimen is the main failure area, while the sandstone remains relatively intact, and no obvious cracks appear on its surface. Due to the superposition of gravity and the weight of the upper rock layer, the microcracks in the failure area continue to occur, and the crack resistance at the rock-coal interface makes the crack unable to penetrate the interface and extend to the sandstone. The surface of the coal specimen of the A ~ D composite is mostly tensile cracks, and its failure (Alper Kirmaci *et al*. 2020) is mainly tensile failure. The local failure is formed by the spalling of large coal blocks at the coal specimen of the composite, and the axial cracks are more developed. The coal specimens of E ~ F composite are subjected to tensile and shear mixed failure, and the edge of the composite coal specimen is peeled off, accompanied by coal splashing and particle ejection, resulting in a large sound. During the compression process of the composite, the rock and coal continuously store elastic energy, and when the specimen reaches the ultimate strength, the coal specimens near the two sides of the rock-coal interface and the coal body at both ends of the bottom appear more serious dislocation damage, and some coal slices are separated from the main body. With the increase of the proportion of rock mass (i.e., h increases), the separation of coal slices on both sides of the coal body is more severe. This is because the elastic energy stored in

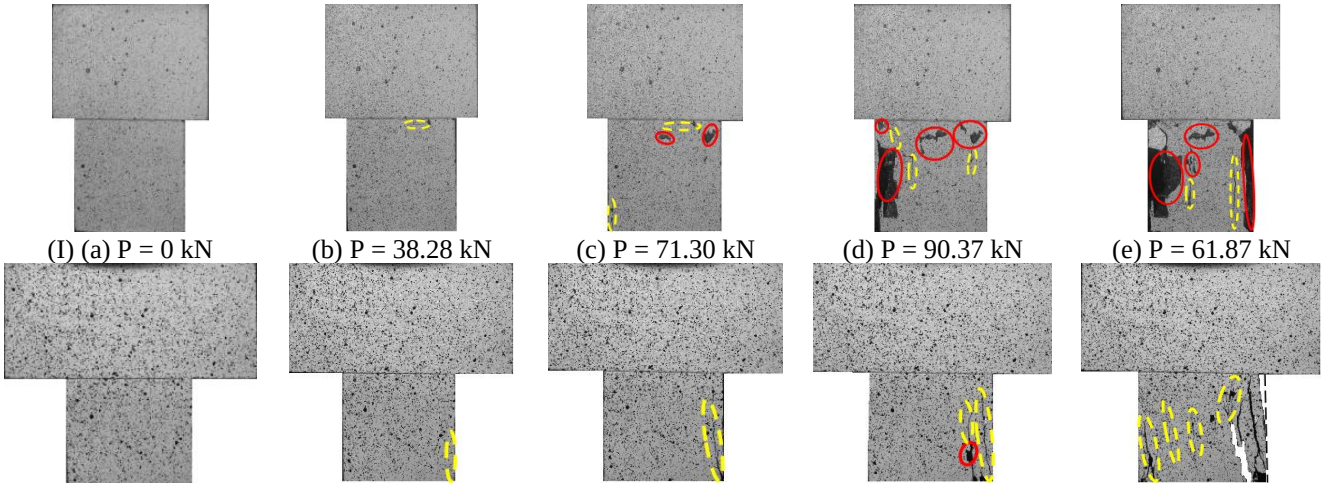

Fig. 6 Progressive failure diagram of rock-coal composite specimen

the rock mass after reaching the peak load is released into the coal body and finally converted into kinetic energy. The larger the proportion of rock mass is, the greater the kinetic energy of coal body in the process of stress impact is, and the more obvious the collapse of coal slices on both sides of coal body is. With the increase of h, the failure mode of the composite changes from tensile failure to mixed tensile-shear failure, and the intensity of the ejection failure of the specimen shows an increasing trend.

The B-2 and F-3 rock-coal assemblage specimens were taken as examples to analyze the uniaxial compression progressive damage characteristics of the assemblage specimens, as shown in Fig. 6. Among them, the yellow ellipse is the newborn crack, the red ellipse is the coal spalling, and the white area of the assemblage is the missing part of the coal specimen after the ejection damage. At the initial stage of loading, the sandstone, coal specimens and their interfaces of B-2 composite specimens were gradually compacted. As the axial pressure increases, a certain degree of micro-cracks in the coal specimen form and expand, and macro-cracks appear on the surface of the coal specimen, that is, the corresponding load P = 38.28kN; as the axial pressure was further increased, the macroscopic cracks continued to develop, increased in number and accompanied by coal block spalling. The moment before the final destabilization of the composite, the initiation crack continues to develop, the stress concentration degree at the crack increases, some dominant cracks expand (Najimi *et al*. 2023) or some dominant cracks in some directions intersect, and the spalling area of the coal block expands, and the coal column becomes unstable when the crack tip searches for a weak surface (Zhang *et al.* 2022), which prompts the assemblage specimen to be destroyed.

The elastic energy stored in the sandstone of the assemblage is released, which leads to the spalling of the assemblage coal specimen, and ultimately destabilization damage occurs. F-3 specimen from loading to destruction, under the influence of bending, macro cracks appeared on both sides of the assemblage coal sample, and the cracks

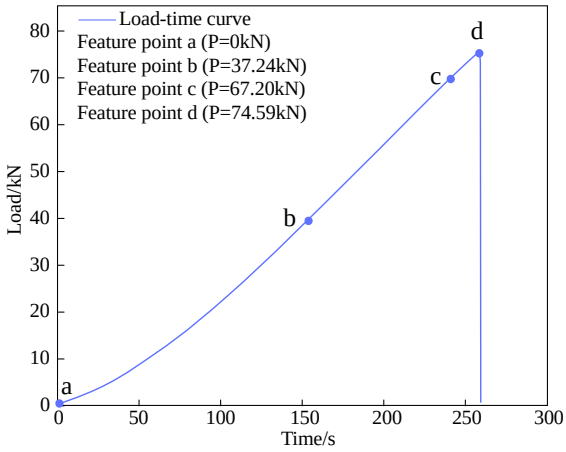

Fig. 7 Selection of load-stroke characteristic points of A-3 composite specimen

were further developed and expanded so that the width increased, and during the period of the spalling of the coal block; the axial pressure continued to increase, and the cracks were rapidly developed and penetrated, and the sandstone on the top released the elastic energy gathered, and a large number of coal chips were ejected and flew out of the assemblage. A large number of coal chips were ejected and flew out, the loaded area of the coal body was reduced, and the assembled body was damaged by spalling-ejecting mixture, and the overall structure of the assembled body specimen was destabilized.

In this uniaxial compression test of non-equal-size rock-coal composite specimens, one specimen was selected for each group to analyze the evolution characteristics of deformation field. Four feature points were taken to show the strain cloud diagram during the loading process, and the deformation and crack propagation process of the specimen were recorded and analyzed, as shown in Fig. 7 (feature point a was selected in the initial state, and feature points b, c and d were respectively in the later stage of compaction stage, the middle stage of elastic deformation stage and the

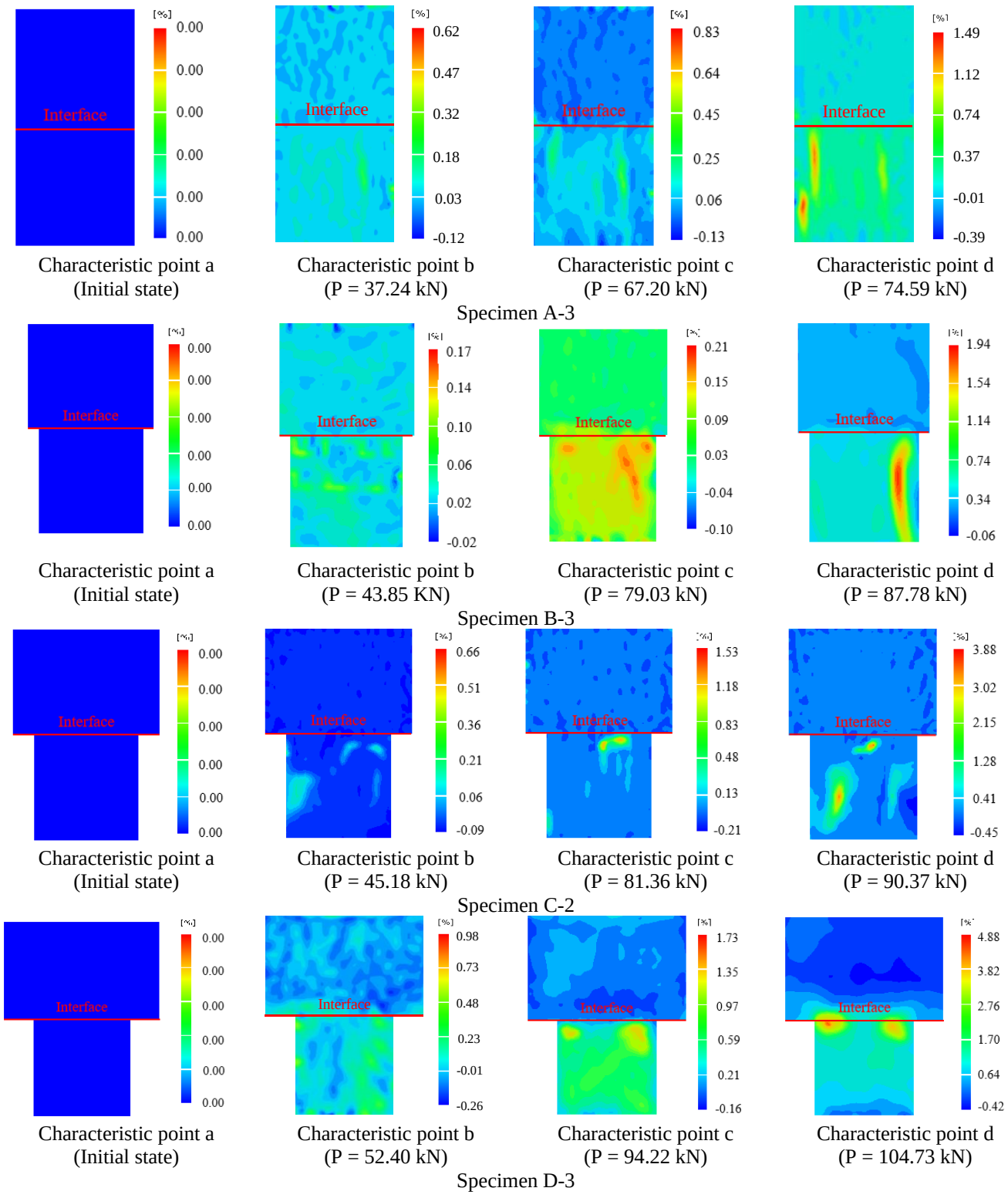

Fig. 8 The maximum principal strain field evolution cloud diagram of non-equal-size rock-coal composite specimen

As can be seen from the figure, the characteristic point a is the initial state of the specimen, within the compaction stage (characteristic point b), the rock-coal composite is in the initial stage of loading under compression, the micro-cracks within the composite are compressed and closed, and the strain near the micro-cracks is relatively large, and at this time, the strain field is approximately uniformly distributed, and the amount of deformation is small. When the composite specimen enters into the elastic deformation stage, the strain field at this time begins to appear strain localization area. Among them, B-3, D-3, E-1 and F-2 specimens show strain localization at both ends of the rock-

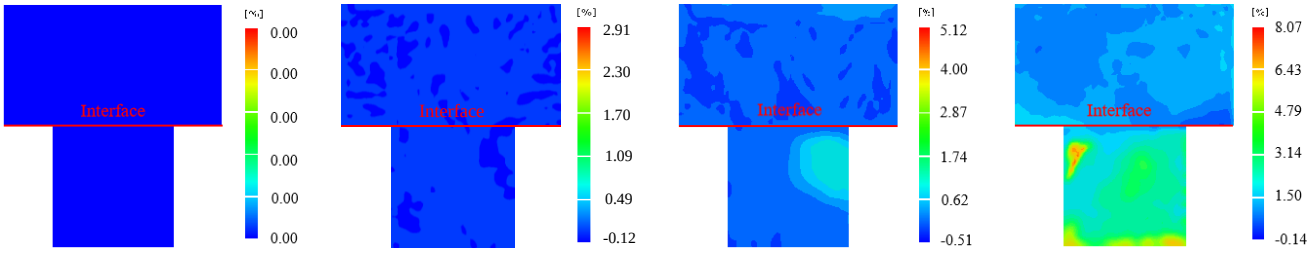

Characteristic point a (Initial state) | Characteristic point b (P = 68.14 kN) | Characteristic point c (P = 122.72 kN) | Characteristic point d (P = 136.34 kN)

Specimen E-1

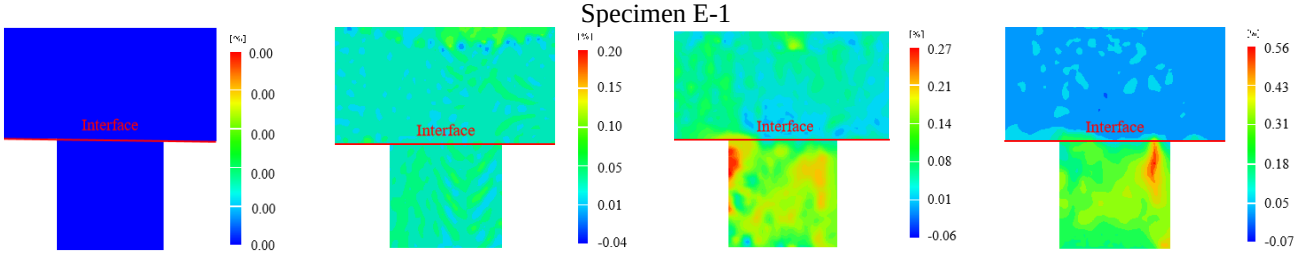

Characteristic point a (Initial state) | Characteristic point b (P = 28.55 kN) | Characteristic point c (P = 51.39 kN) | Characteristic point d (P = 57.10 kN)

Specimen F-2

Fig. 8 Continued-

coal interface. At this time, new cracks gradually develop, and differential deformation occurs at each point on the surface of the specimen. The larger and smaller strain differences in the strain field begin to appear, and the strain values at both ends of the rock-coal interface are larger. This is caused by the "size effect" and "bending effect" between coal and rock. As a kind of rock mass containing primary defects, coal will produce stress concentration at the defects under the action of axial pressure, thus changing its internal stress field distribution. At the same time, due to the existence of irregular sizes in this test, the composite specimens without supporting structures on both sides produce "bending" deformation under the action of external force-bending moment, resulting in the formation of weak areas at both ends of the rock-coal interface, where strain localization areas are more likely to occur. The strain localization phenomenon occurs at the primary crack of the coal specimen in the A-3 and C-2 specimens, where the strain value is large, and the crack penetrates the whole coal seam after the loading. At the characteristic point d, the internal crack of the specimen enters the unstable development stage, and the deformation difference of each point on the surface of the specimen is prominent. The high strain concentration phenomenon appears in the red area of the graph, and the strain field appears at both ends of the rock-coal interface. Large strain concentration area. The deformation and destruction of the specimen is accompanied by the release of elastic energy, and the released elastic energy maintains the further expansion of the cracks. Under the action of axial pressure, the tip of the primary crack in the coal sample cracked and expanded to form a macro tension crack, and the length and width of the crack increased.

The evolution law of the strain field of the combined specimen shows that with the increase of h, the strain concentration area of the composite changes from uniform distribution to both ends of the rock-coal interface during the axial pressure loading process, and a weak area is easily formed there, accompanied by a certain degree of internal micro-crack formation and expansion. When the strain at this place shows a more obvious increasing trend, it shows that the micro-cracks inside the combined coal specimen at this stage rapidly expand to macro-cracks.

In order to further study the effect of "bending" deformation on the specimen of rock-coal composite, three monitoring points were set up at the sandstone and coal specimen of rock-coal composite. As shown in Fig. 9, the measuring point 1 is located at 25 mm from the upper end of the specimen and 23 mm on the left side of the center line. The measuring point 2 is located at 25 mm from the upper end face of the specimen and the center line, and the measuring point 3 is located at 25 mm from the lower end face of the specimen and 23 mm from the left side of the center line.

In order to further explore the influence of the width ratio of rock and coal on the bearing capacity of the combined sample, according to the above key measuring point position, the displacement monitoring and analysis work at the measuring point of each combined sample is carried out. Fig. 10 gives the evolution curve of the vertical displacement of the measuring point of the combined sample. Fig. 11 is the evolution curve of the difference between the maximum vertical displacement of the measuring point 1 and 2. During the loading period, the measuring point 3 of the six groups of composite samples is relatively stable, and the fluctuation range is slightly smaller, while the vertical displacement of the measuring points 1 and 2 has a significant change. In the initial stage of loading, the vertical displacement of measuring points 1 and 2 increases at the same rate. With the increase of load,

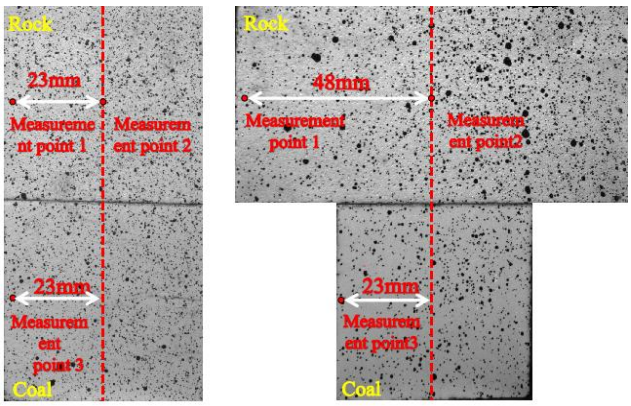

Fig. 9 Arrangement of monitoring points

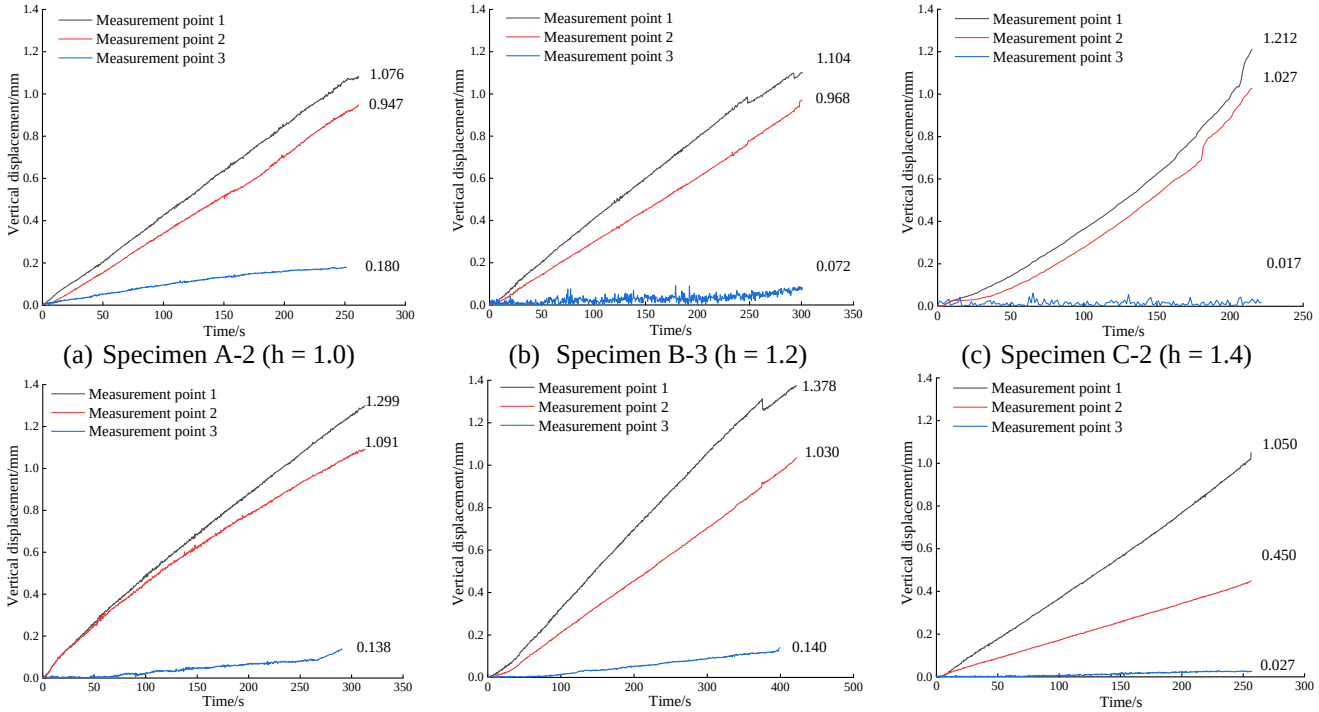

(a) Specimen A-2 (h = 1.0) (b) Specimen B-3 (h = 1.2) (c) Specimen C-2 (h = 1.4)

(d) Specimen D-1 (h = 1.6) (e) Specimen E-1 (h = 1.8) (f) Specimen F-2 (h = 2.0)

Fig. 10 The vertical displacement evolution curve of the monitoring point of the combined specimen

the growth rate of vertical displacement of measuring point 1 exceeds that of measuring point 2, especially the growth rate of group F is the fastest.

The deformation of the measuring points at the sandstone and coal samples is not synchronized, which is caused by the difference in the mechanical properties of the sandstone and coal samples. The deformation of measuring point 1 and measuring point 2 at sandstone is not synchronized, which is caused by the "bending" deformation of the sample. When h is 1.0 ~ 1.6, the difference between measuring points 1 and 2 in groups A ~ D is small, and the phenomenon of "bending" is relatively not obvious. At this time, the compression effect of the sample is more prominent. The increase of the bearing area of the structure on both sides of the sandstone makes it possible to share more loads borne by the main bearing structure coal sample, thus reducing the damage effect of the axial pressure on the main bearing coal sample and improving the overall bearing capacity of the composite sample accordingly. When h increases to 1.8, the difference between measuring points 1 and 2 in group E begins to increase, and the "bending" phenomenon gradually becomes obvious, but the compression deformation behavior still dominates. Therefore, when h is 1.0 ~ 1.8, as h increases, the bearing capacity of the sample is improved, and the peak load also increases. When h increases to 2.0, the difference between measuring points 1 and 2 in group F is large, and the phenomenon of "bending" is very obvious.

At this time, the "bending" deformation plays a decisive role, which has a significant deterioration effect on the combination, resulting in a decrease in the bearing capacity of the sample in group F, which aggravates the instability and failure of the combination, thus minimizing the peak load of the sample.

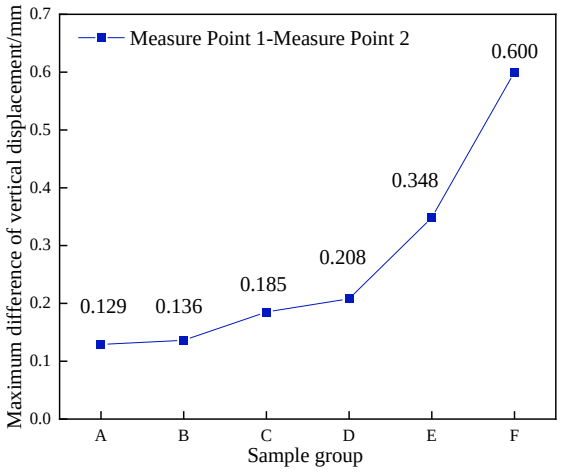

Fig. 11 The evolution curve of the maximum difference of vertical displacement between measuring points 1 and 2

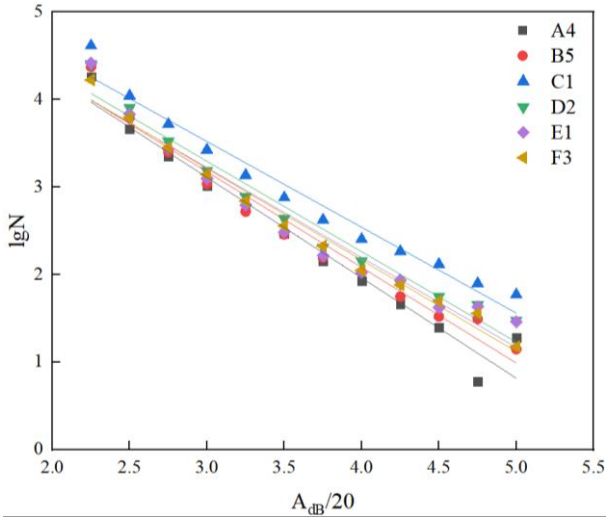

Fig. 12 Acoustic emission amplitude-frequency distribution diagram of non-equal-size rock-coal composite specimen

3.3 Evolution law of acoustic emission of rock-coal composite

The acoustic emission signal can reflect the crack development and evolution law inside the rock-coal composite in the process of load damage and destruction of the composite. Among them, the acoustic emission (AE) b value (Hu *et al.* 2023) is an important parameter in the acoustic emission test. Its physical meaning is the ratio of the number of small events to the number of large events in the process of rock fracture, which can better reflect the internal crack propagation in the process of rock fracture instability. When the b value is large, it corresponds to a large number of small events, and when the b value is small, it corresponds to a large number of large events. The increase of b value indicates that the acoustic emission activity of the specimen is enhanced during the loading process and is dominated by small-scale micro-fracture. The decrease of b value indicates that the acoustic emission activity of the specimen is weakened during the loading process, but accompanied by the generation of large-scale cracks or the sharp increase of crack propagation speed. When the b value is constant, the distribution of large and small scale micro-fracture phenomena in the specimen is balanced.

Referring to the b value of seismology, combined with G-R formula and acoustic emission data, the b value of acoustic emission can be calculated. The formula is as follows

$$\lg(N) = a - bM \tag{1}$$

$$M = \frac{A_{dB}}{20} \tag{2}$$

In the formula, N is the number of earthquakes ; M is the magnitude ; A_{dB} is the amplitude of acoustic emission ; a and b are constants.

Select ΔA_{dB} = 5 dB to calculate the acoustic emission amplitude data, and use the least square method to calculate the data.

Table 2 is the statistical table of acoustic emission b value and fitting degree R2 of non-equal-size rock-coal composite specimens, and Fig. 12 is the acoustic emission amplitude-frequency distribution diagram of representative specimens of non-equal-size rock-coal composite. It can be seen from Table 2 and Fig. 12 that under different rock and coal width ratios, the acoustic emission amplitude-frequency distribution of the combined specimen shows a good linear relationship, and the fitting degree R^2 is higher than 0.9, which conforms to the G-R relationship (Gutenberg *et al.* 1944).

In order to further study the variation law of acoustic emission in the progressive failure of the composite body, A-1, B-1, C-2, D-2, E-3 and F-2 composite specimens were selected, and the dynamic b value of acoustic emission was used as the parameter. The specific calculation method is : 3000 AE events are selected as the calculation window, and the number of AE events per 1500 AE events is the step size, and the variation characteristics of the acoustic emission b value during the failure process of the composite specimen are obtained. Fig. 13 shows the load-ringing count-dynamic b-value evolution curve of non-equal-size rock-coal composite specimens with time.

As can be seen from Fig. 13, the load-time curve of the rock-coal composite mainly includes three stages : compaction (initial point ~ point a), linear elasticity (point a ~ point c), and post-peak steep drop (point c ~ termination point). With the loading of axial stress, the acoustic emission count signal of the composite specimen has obvious periodic changes, and according to the number and fluctuation frequency of the acoustic emission count signal, the progressive failure process of the composite specimen under uniaxial compression is divided into four stages: calm stage (initial point ~ point a), fluctuation rising stage (point a ~ point b), growth stage (point b ~ point c) and steep increase stage (point b ~ point c). Meanwhile, the acoustic emission signal characteristics and the load-time curve show good consistency during the loading process of the rock-coal composite.

Table 2 Statistical table of acoustic emission b value of non-equal-size rock-coal composite specimens

Groups	h	Value type	b-value	R^2
Group A	1.0	Min. ~ Max.	0.8852 ~ 1.1471	0.9433 ~ 0.9642
		Average value	0.1072	0.9568
Group B	1.2	Minimum ~ Maximum	0.9852 ~ 1.0931	0.9392 ~ 0.9688
		Average value	1.0417	0.9573
Group C	1.4	Minimum ~ maximum	0.8884 ~ 0.1198	0.9512 ~ 0.9675
		Average value	0.9604	0.9570
Group D	1.6	Minimum ~ maximum	0.8657 ~ 1.0328	0.9044 ~ 0.9665
		Average value	0.9533	0.9393
Group E	1.8	Minimum ~ maximum	0.7734 ~ 1.0260	0.9265 ~ 0.9491
		Average value	0.8800	0.9352
Group F	2.0	Minimum ~ maximum	0.9483 ~ 1.0465	0.9073 ~ 0.9847
		Average value	0.9285	0.9559

(1) In the calm stage (initial point ~ point a), the composite specimen is in the pressure-tight stage, with only a few or even no acoustic emission events, and the number of ringing counts is small and grows slowly. At this stage, the energy is in the accumulation period, the proportion of small-scale cracks inside the composite specimen starts to increase, and the external load is small enough to make the primary cracks expand or produce new cracks. The acoustic emission b-value of the composite specimen is large and shows a small growth trend, indicating that at this time the composite specimen generated mostly small events within the composite specimen, microcracks develop slowly and stably, and the proportion of large events is low..

(2) The fluctuating rising stage (point a~point b), the acoustic emission signal is gradually active, there are fine joints inside the assemblage, and the acoustic emission events are due to crack closure and so on. The energy in this stage accumulates, and the ringing count enters the growth period. The microcracks are continuously compacted, the initial cracks of the specimen begin to develop and expand, and the b-value decreases; the acoustic emission signal is active to some extent, and the b-value floats slightly around 1, indicating that at this time, the small and large events generated within the assemblage specimen account for the same proportion.

(3) In the growth stage (point b~point c), the acoustic emission events are active, and the acoustic emission ringing count intensity and frequency increase significantly compared with the calm stage and the growth stage, and with the increase of h, the acoustic emission ringing count signals increase abruptly when the assembled specimen is in the late stage of uniaxial loading, and the assembled specimen undergoes the prolongation of the overall damage time. At this stage, the primary cracks of the combined body specimen expand, newborn cracks are generated, and the damage degree of the combined body coal specimen increases. With the loading of axial stress, when the elastic energy accumulated inside the assembled body specimen exceeds the limit, the cracks will rapidly expand and develop, and when the axial stress is close to the peak load, the original and newborn cracks break through the last obstacle to intersect and pass through, and the assembled body coal specimen suddenly releases the energy inside the assembled body and undergoes damage. At the same time, the dynamic b-value of the 6 groups of assemblage samples in this stage decreases substantially, at this time, the high-energy acoustic emission events occur continuously, the proportion of which begins to increase, and the development of large-scale cracks changes drastically, and the decrease in b-value near the peak load can be used as a precursor information for the impending instability of the rock-coal assemblage samples.

(4) Steep increase stage (point c~termination point), which lasts for a very short time and reaches peak counts at this stage. Under the action of axial stress, the connection between some crystal particles inside the assemblage is destroyed, and the energy accumulated during the loading process is continuously released, resulting in the maximum damage of the assemblage specimen within a unit of time, and the acoustic emission ringing count reaches the maximum value. Since the micro-damage to the final damage, the dynamic b-value decreases continuously, the dynamic b-value of A-1 specimen decreases by 0.42, and the b-value of B-1, C-2, D-2, E-3 and F-2 specimens decreases by 0.48, 0.56, 0.60, 0.76, 0.91, respectively, and the b-value decreases by an enlarged magnitude, which indicates that the rock-coal specimen is easier to form penetrations and the large-size cracks are generated during the whole loading process. rate is accelerated throughout the loading process, and it is easier to form a through damage surface.

4. Bearing failure mechanism of rock-coal composite body

In this test, because the strength of sandstone in the combined coal rock is much larger than that of the coal specimen, the coal specimen in the combined coal rock is damaged to varying degrees, while the sandstone is not damaged. Therefore, the coal specimen is the main bearing part of the composite, and the peak load of the rock-coal composite specimen is mainly determined by the peak load of the coal specimen. In order to reveal the bearing failure mechanism of non-equal-size rock-coal composite, the load-bearing failure model of rock-coal composite is established as shown in Fig. 14.

The failure mechanism of rock-coal combination is mainly reflected in two aspects : first, the sharing effect of cantilever structure on both sides of sandstone on the

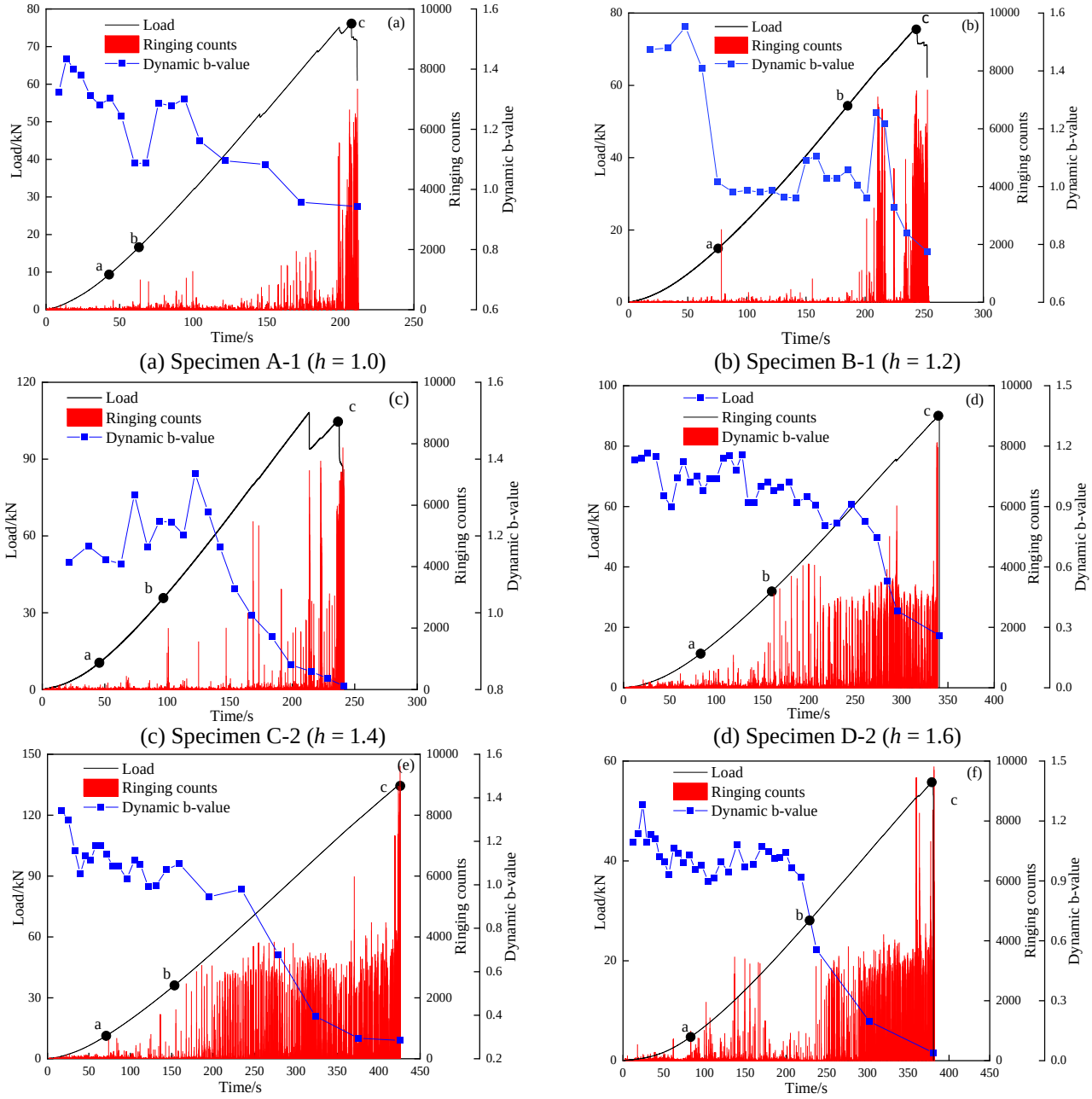

(a) Specimen A-1 (h = 1.0) (b) Specimen B-1 (h = 1.2)

(c) Specimen C-2 (h = 1.4) (d) Specimen D-2 (h = 1.6)

(e) Specimen E-3 (h = 1.8) (f) Specimen F-2 (h = 2.0)

Fig. 13 The load-ringing count-dynamic b value evolution curve of non-equal-size rock-coal composite specimen

overall bearing capacity of the combination specimen ; second, the cantilever structure on both sides of the sandstone produces bending deformation under axial load, which weakens the overall bearing capacity of the composite specimen.

When the test machine is loaded, the axial stress indirectly acts on the coal sample through the sandstone, and the sandstone and the coal sample are compressed and deformed. As h increases, the bearing area of the structure on both sides of the sandstone increases, which can share part of the load borne by the main bearing structure coal sample. To a certain extent, the ability of the coal sample to resist deformation is enhanced, so that the whole composite sample can better adapt to the increase of axial stress, improve the bearing capacity of the coal sample, and finally improve the overall bearing capacity of the composite sample. Therefore, when the rock and coal width ratio h is 1.0 ~ 1.8, the peak load of the A ~ E combination specimens shows an increasing trend.

As h further increases to 2.0, although the structural bearing area S on both sides of the sandstone can share part of the load borne by the coal sample, this sharing effect has a certain limit. At this time, the structure on both sides of the sandstone forms a bending moment under the action of axial load and then produces a “bending” deformation, which changes the stress concentration position of the combined specimen. In the whole process of failure of the combined specimen, the micro-crack nucleation

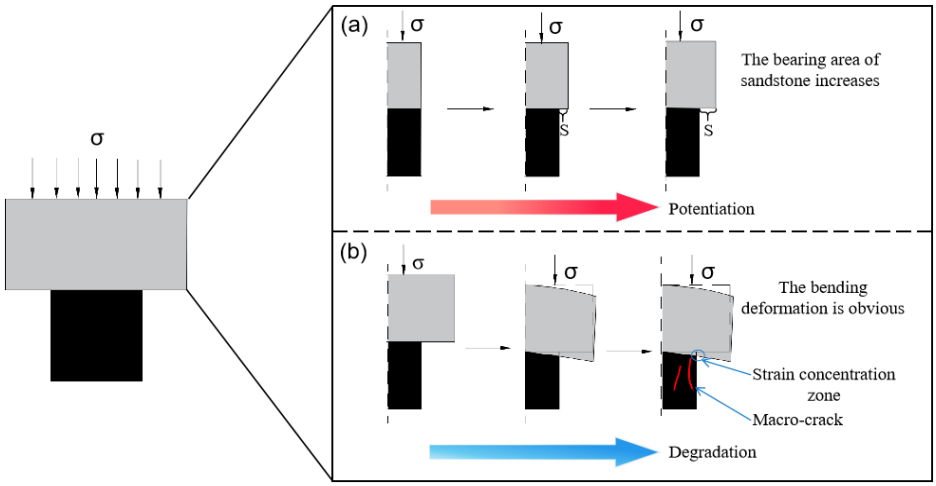

Fig. 14 Bearing failure model of rock-coal composite body

phenomenon caused by stress concentration will form a local strain band at the crack tip at both ends of the rock-coal interface, and finally form a macro-crack. Combined with the macroscopic morphology of the typical combination under unequal size, it can be seen that during the compression process of the combination, the rock and coal continuously store elastic energy, and the elastic energy in the coal body first reaches its energy storage limit. The macroscopic cracks expand and penetrate, and the coal sample produces macroscopic damage. At this time, the energy accumulated inside the rock mass is released, which in turn aggravates the damage degree of the combination and the possibility of instability and failure.

In summary, with the increase of the width ratio of rock to coal, the bearing area S on both sides of the sandstone increases, and the part of the load borne by the coal sample increases, thus improving the bearing capacity of the coal sample. However, this effect is limited. When h increases to 2.0, the "bending" deformation effect is prominent, which aggravates the damage of the combined coal sample and reduces the bearing capacity of the combined body. At the same time, with the increase of the proportion of rock mass (i.e., h increases), the stronger the ability of sandstone to share part of the load of coal sample, the more energy stored. When the sample reaches the ultimate load, the coal sheets on both sides of the coal body appear more serious dislocation damage, accompanied by some coal sheets separated from the main body. The destruction of the coal sample induces part of the energy released by the sandstone, which causes the coal sheets on both sides of the coal sample to separate more violently. The less the loaded area of the coal body, which leads to a significant decrease in the bearing capacity of the combination and a greater degree of fragmentation.

5. Conclusions

(1) With the increase of the width ratio h between rock and coal, the peak load of the non-equal-size rock-coal specimen shows a trend of increasing and then decreasing. The peak loads of the rock-coal assemblage specimens are larger than those of the single coal specimens and smaller than those of the single sandstone specimens. Compared with the square-column-shaped group A specimens, the average peak loads of non-equal-sized group B, C, D and E specimens increased by 10.61%, 15.09%, 34.69% and 67.37%, respectively, and the average peak loads of group F specimens decreased by 22.91%.

(2) The failure of the combined specimen mainly occurs in the coal specimen, and the sandstone has not been significantly damaged. With the increase of h, the composite specimen is more likely to form a weak area at both ends of the rock-coal interface. The failure mode of the composite changes from spalling failure to spalling-ejection mixed failure, and the degree of fragmentation becomes more obvious.

(3) The acoustic emission characteristic signals of rock-coal composite specimens can be divided into four stages : calm, fluctuating rising, growth and steep increase. As h increases, the acoustic emission signal of the composite is more obvious, and the overall failure time of the specimen is prolonged. The acoustic emission amplitude-frequency distribution of the rock-coal composite specimens showed a good linear relationship, and the dynamic b value decreased significantly at the later stage of loading. The decrease of the b value near the peak load can be used as a precursory information for the instability of the rock-coal composite.

(4) When the width ratio of rock to coal is 1.0 ~ 1.8, with the increase of h, the bearing area of the structure on both sides of the sandstone increases, which can share part of the load borne by the coal specimen of the main bearing structure and improve the overall bearing capacity of the composite specimen. However, this effect is limited. As h further increases to 2.0, the "bending" deformation effect is prominent, which has a more obvious deterioration effect on the composite, reduces the bearing capacity of the composite, and aggravates the damage of the coal specimen of the composite.

Acknowledgements

This work was supported by the National Natural Science Foundation of China (Grant Nos. 52274128), and

the Open Fund Research Project, supported by the State Key Laboratory of Mining Response and Disaster Prevention and Control in Deep Coal Mines (Grant No. SKLMRDPC22KF01). This work was supported by the Taishan Scholars Project Special Fund (NO.tsqn202306199).

References

Atsushi, S. and Hani, S.M. (2017), "Numerical investigation into pillar failure induced by time-dependent skin degradation", *Int. J. Min. Sci. Technol.*, **27**(4), 591-597. https://doi.org/10.1016/j.ijmst.2017.05.002.

Chen, G.B. Zhang J., Li, Y., Liu, F.X., Li, T. and Zhang, G.H. (2022), "Energy distribution law of coal–rock combined body under confining pressure effect", *Acta Geophys*., **71**(4), 1831-1843. https://doi.org/10.1007/S11600-022-00968-4.

Chen, S.J., Qu, X., Yin, D.W., Liu, X.Q., Ma, H.F. and Wang, H.Y. (2018), "Investigation lateral deformation and failure characteristics of strip coal pillar in deep mining", *Geomech. Eng*., **14**(5), 421-428. https://doi.org/10.12989/gae.2018.14.5.421.

Chen, S.J., Yin, D.W., and Jiang, N., Wang, F. and Guo, W.J. (2019b), "Simulation study on effects of loading rate on uniaxial compression failure of composite rock-coal layer", *Geomech. Eng*., **17**(4), 333-342. https://doi.org/10.12989/gae.2019.17.4.333.

Chen, S.J., Yin, D.W., Liu, H.M., Chen, B. and Jiang, N. (2019a), "Effects of coal's initial macro-cracks on rockburst tendency of rock-coal composite samples", *Royal Soc. Open Sci*., **6**(11), 181795, https://doi.org/10.1098/rsos.181795.

Chen, Y.L., Zuo, J.P., Liu, D.J. and Wang, Z.B. (2019), "Deformation failure characteristics of coal-rock combined body under uniaxial compression: experimental and numerical investigations", *Bull. Eng. Geol. Environ*., **78**(5), 3449-3464. https://doi.org/10.1007/s10064-018-1336-0.

Gao, W. and Ge, M.M. (2016), "Stability of a coal pillar for strip mining based on an elastic-plastic analysis", *Int. J. Rock. Mech. Min*., **87**, 23-28. https://doi.org/10.1016/j.ijrmms.2016.05.009.

Gutenberg, B. and Richter, C.F. (1944), "Frequency of earthquakes in California", *Bull. Seismol. Soc. Am*., **34**(4), 185-188. https://doi.org/10.1785/BSSA0340040185.

Hu, S.C., Zhou, X.D., Ru, W.K., Han, J.M., Guo, S.H., Zhang, C.X. and Yang, L. (2023), "Study on mechanical property of coal-rock combination under different unloading confining pressure rate", *Geotech. Geol. Eng*., **41**(4), 2629-2644. https://doi.org/ 10.1007/S10706-023-02417-5.

Hu, S.H. Su, G.S., Qin, Y.Z. and Jiang, J.Q. (2023), "Influence of the loading rate on the evolution characteristics of AE and MS signals during granite failure", *Eng. Fail. Anal*., **152**, 107428. https://doi.org/10.1016/j.engfailanal.2023.107428.

Jiang, Y.J., Liang, B., Wang, D., Luan, H.J., Zhang, G.C., Dong, L. and Chen, L.G. (2024), "Experimental study on failure mechanical properties and acoustic emission characteristics of soft rock-coal combination under dynamic disturbance", *Eng. Fail. Anal*., **158**, 108016. https://doi.org/10.1016/j.engfailanal.2024.108016.

Jin, P.J., Wang, E.Y. and Song, D.Z. (2017), "Study on correlation of acoustic emission and plastic strain based on coal-rock damage theory", *Geomech. Eng*., **12**(4), 627-637. https://doi.org/10.12989/gae.2017.12.4.627.

Kabiesz, J., Lurka, A. and Drzewiecki, J. (2015), "Selected methods of rock structure disintegration to control mining hazards" . *Arch. Min. Sci*., **60**(32), 807-824. https://doi.org/10.1515/amsc-2015-0053.

Kirmaci, A. and Erkayaoglu, M. (2020) "Thermographic analysis of failure for different rock types under uniaxial loading", *Geomech. Eng*., **23**(6), 503-512. https://doi.org/10.12989/gae.2020.23.6.503.

Lei, S., Hao, D.Y. and Cao, S.W. (2023), "Study on uniaxial compression deformation and fracture development characteristics of weak interlayer coal–rock combination", *Fractal Fract*., **7**(10), 731. https://doi.org/10.3390/fractalfract7100731.

Li, F.X., Yin, D.W., Wang, F., Jiang, N. and Li, X.L. (2022), "Effects of combination mode on mechanical properties of bi-material samples consisting of rock and coal", *J. Mater. Res. Technol*., **19**, 2156-2170, https://doi.org/10.1016/j.jmrt.2022.05.174.

Li, X.P., Li, X.S., Yuan, H.H., Li, H.T., Yang, G.Y., Wang, S.W., Ding, G.L. and Su, S.J. (2024), "The failure behavior of coal-rock combined body under compression-shear loading", *Sci. Progress*, **107**(1). https://doi.org/10.1177/00368504231225860..

Liu X.S., Tan Y.L., Ning J.G., Lu, Y.W. and Gu, Q.H. (2018), "Mechanical properties and damage constitutive model of coal in coal-rock combined body", *Int. J. Rock Mech. Min. Sci*., **110**, 140-150. https://doi.org/10.1016/j.ijrmms.2018.07.020..

Liu, J.W., Wu, N., Si, G.Y. and Zhao, M.X. (2021), "Experimental study on mechanical properties and failure behaviour of the pre-cracked coal-rock combination", *Bull. Eng. Geol. Environ*., **80**(3), 2307-2321. https://doi.org/10.1007/s10064-020-02049-6.

Liu, Y., Chen, B., Cui, S.L. and Yin, D. (2022), "Similar simulation test on deformation characteristics of overlying rock developed by instability of strip coal pillar", *Shock Vib*., **2022**, 4470851. https ://doi.org/10.1155/2022/4470851.

Lv, K., Jiang, N., Yin, D.W., Meng, S.Y., Gao, Z.Y. and Lv, T. (2024), "Deterioration of compressive properties of coal rocks under water and gas coupling", *J. Cent. South Univ*., **31**(2), 475-493. https://doi.org/10.1007/s11771-024-5583-x.

Ma, Q., Tan, Y.L., Liu, X.S., Gu, Q.H. and Li, X.B. (2020), "Effect of coal thicknesses on energy evolution characteristics of roof rock-coal-floor rock sandwich composite structure and its damage constitutive model", *Compos. Part B-Eng*., **198**, 108086. https://doi.org/10.1016/j.compositesb.2020.108086.

Ma, S.Z., Liu, K.W., Guo, T.F., Yang, J.C., Li, X.D. and Yan, Z.X. (2022), "Experimental and numerical investigation on the mechanical characteristics and failure mechanism of cracked coal & rock-like combined sample under uniaxial compression", *Theor. Appl. Fract. Mech*., **122**, 103583. https://doi.org/10.1016/j.tafmec.2022.103583.

Marasanov, V., Sharko, A., Sharko A. and Stepanchikov. D. (2019), "Modeling of energy spectrum of acoustic-emission signals in dynamic deformation processes of medium with microstructure", *Proceedings of the IEEE 39th International Conference on electronics and nanotechnology (ELNANO)*, 718-723. https://doi.org/10.1109/ELNANO.2019.8783809.

Najimi, M. and Aboutalebi, FH. (2023), "Mixed Mode Crack Initiation and Propagation in Functionally Graded Materials: Experimental and Numerical Investigations", *IJST-T Mech. Eng.*, **47**(4), 1829-1839. https://doi.org/10.1007/s40997-023-00591-8.

Petukhov, I.M. and Linkov, A.M. (1979), "The theory of post-failure deformations and the problem of stability in rock mechanics", *Int. J. Rock Mech. Min. Sci*., **16**(2), 57-76. https://doi.org/10.1016/0148-9062(79)91444-X.

Sinha, S. and Walton, G. (2021) "Investigation of pillar damage mechanisms and rock-support interaction using Bonded Block Models", *Int. J. Rock Mech. Min. Sci*., **138**(104652), 1365-1609. https://doi.org/10.1016/j.ijrmms.2021.104652.

Vinay, L.S., Bhattacharjee, R.M., Ghosh, N., Budi, G., Kumar, J. V. and Kumar, S. (2022), "Numerical study of stability of coal pillars under the influence of line of extraction", *Geomat. Nat. Haz. Risk*., **13**(1), 1556-1570. https://doi.org/10.1080/19475705.2022.2088409.

Xue, J.H., Chen, Z.H., Li, Y.H., Wang, J.Y. and Li, X. (2022), "Failure characteristics of coal-rock combined bodies based on acoustic emission signals", *Arabian J. Geosci*., **15**(2), 135. https://doi.org/10.1007/S12517-021-09419-8.

Yin, D.W., Chen, S.J., Chen. B., Liu, X.Q. and Ma, H.F. (2018), "Strength and failure characteristics of the rock-coal combined body with single joint in coal", *Geomech. Eng*., **15**(5), 1113-1124. https://doi.org/10.12989/gae.2018.15.5.1113.

Yin, D.W., Ding, Y.S., Jiang, N., Li, F.X., Zhang, J.C. and Xu H.H. (2022), "Mechanical properties and damage characteristics of coal samples under water immersion pressure", *Lithosphere*, **2022**(1), 1278783. https://doi.org/10.2113/2022/1278783.

Zhang, C., Zhao, Y.X., Han, P.H. and Bai, Q.S. (2022), "Coal pillar failure analysis and instability evaluation methods: A short review and prospect", *Eng. Fail. Anal*., **138**, 106344. https ://doi.org/10.1016/j.engfailanal.2022.106344.

Zhang, Y.J., Cui, B.Y., Wang, Y.N., Zhang, S., Feng, G.R. and Zhang, Z.J. (2023), "Evolution law of shallow water in multi-face mining based on partition characteristics of catastrophe theory", *Fractal. Fract*., **7**(11), 779. https://doi.org/10.3390/fractalfract7110779.

Zhao, T.B., Guo, W.Y., Lu, C.P. and Zhao, G.M. (2016), "Failure characteristics of combined coal-rock with different interfacial angles", *Geomech. Eng*., **11**(3), 345-359. https://doi.org/10.12989/gae.2016.11.3.345.

Zhao, W.H., Huang, R.Q. and Yan, M. (2015), "Mechanical and fracture behavior of rock mass with parallel concentrated joints with different dip angle and number based on PFC simulation", *Geomech. Eng*., **8**(6), 757-767. https://doi.org/10.12989/gae.2015.8.6.757.

Zuo, J.P., Chen, Y. and Liu, X.L.(2019) "Crack evolution behavior of rocks under confining pressures and its propagation model before peak stress", *J. Cent. South Univ*., **26**(11), 3045-3056. https://doi.org/10.1007/S11771-019-4235-Z.

GC